

DEGRADATION EFFECTS OF SOLAR RADIATION ON THE MECHANICAL PROPERTIES OF COMPOSITE MATERIALS: AN EXPERIMENTAL INVESTIGATION

JINDRICH VILIS¹, PAVEL SAFL², BUI THANH PHAN¹, JAN ZOUHAR³, ZDENEK POKORNY¹, ONDREJ LINKA¹

¹University of Defence, Faculty of Military Technology, Department of Mechanical Engineering, Kounicova 65, 662 10 Brno, Czech Republic

²Brno University of Technology, Faculty of Electrical Engineering and Communication, Technicka 3058/10, 616 00 Brno, Czech Republic

³Brno University of Technology, Faculty of Mechanical Engineering, Technicka 2896/2, 616 69 Brno, Czech Republic

DOI: 10.17973/MMSJ.2025_06_2025056

jindrich.vilis@unob.cz

This study investigates the degradation of the mechanical properties of composite materials based on para-aramid fiber Twaron CT 747 due to prolonged exposure to sunlight. Composite samples were fabricated using three manufacturing technologies: vacuum-assisted resin transfer molding (VARTM), autoclave curing, and hot-pressing. The mechanical properties were characterized through uniaxial tensile testing and flexural tests. The testing included reference samples (unexposed) and samples exposed to sunlight for 31 days and 122 days. The reference samples exhibited tensile strengths of 586.4 MPa (VARTM), 492.8 MPa (autoclave), and 399.6 MPa (hot-pressing). After 122 days of sunlight exposure, tensile strength decreased by 29.6% (VARTM), 35.2% (autoclave), and 45.7% (hot-pressing), with the most significant decline in tensile modulus observed in the hot-pressed samples. Sunlight exposure also led to a reduction in flexural characteristics. Fractography analysis via scanning electron microscopy revealed layer delamination and the formation of microcracks, confirming the adverse effects of sunlight on material integrity. The findings of this study highlight the significant impact of prolonged solar exposure on the mechanical integrity of composite materials intended for outdoor applications.

KEYWORDS

composite, aramid, solar exposure, degradation, mechanical properties

1 INTRODUCTION

In light of the growing demand for materials that offer a combination of low weight and high strength, composite materials have become integral to the aerospace, automotive, space, marine, and sports industries [Sharma 2023, Arulprasanna 2024, Sumithra 2023].

Composites are composed of two or more constituents. Their interaction results in the attainment of specific properties that exceed those of the individual components [Mechali 2024, Saharudin 2021, Chaudhary 2024, Sharma 2020]. The primary components of composite materials are the matrix and the

reinforcement. The matrix is the continuous phase of the composite, which ensures the cohesion of the reinforcing phase. It protects the reinforcement from external influences and maintains the integrity of the composite material [Chaudhary 2024]. The reinforcing phase represents the discontinuous phase of the composite. It plays a critical role in transferring mechanical loads and providing the desired mechanical properties [Sharma 2020]. The most commonly used reinforcements are fiber reinforcements, with the most widespread being glass, carbon, and aramid fibers [Mahboubzadeh 2024, Sajan 2021].

Aramid fibers (Twaron[®], Kevlar[®]) are composed of long molecular chains of the polymer PPTA poly(p-phenylene terephthalamide) [Xiao 2024]. These chains are interconnected through van der Waals forces, hydrogen bonds, and layered interactions between aromatic cores [Xiao 2024, Dharmavarapu 2022]. Aramids are characterized by high tensile strength, low density, and a high modulus of elasticity [Dharmavarapu 2022, Talikoti 2019]. They also exhibit thermal resistance and resistance to a wide range of chemicals [Talikoti 2019]. However, aramid fibers have certain disadvantages. The main drawbacks include their low resistance to UV radiation and moisture [Viliš 2024].

With the increasing use of composite materials, there is a growing need to investigate their mechanical properties under the influence of degradative factors, which has become the subject of numerous research studies. For instance, Santos et al. [Santos 2023] examined the effect of UV sensitivity and accelerated aging on the puncture resistance of textiles made from p-aramid fibers impregnated with Shear Thickening Fluids (STF). The results showed that impregnation with these fluids significantly enhanced the material's resistance to penetration, specifically by up to 81% compared to non-impregnated fibers. The authors also found that UV exposure negatively impacted the mechanical properties of the textiles. Furthermore, it was demonstrated that the interaction between nanoparticles in the STF and the fibers increased friction, thereby enhancing the energy absorption and dissipation mechanisms against impact. Similarly, in the study [Wakatsuki 2022], Wakatsuki et al. focused on the influence of the ratio of m-aramid to p-aramid in fabrics intended for firefighter clothing on their tensile strength under UV exposure. They found that a higher content of p-aramid demonstrated greater resistance to degradation. In this study, they also developed a predictive model that allows for the estimation of tensile strength loss based on the level of UV exposure. These findings suggest the potential for optimizing the ratio of aramid fibers to enhance the lifespan of firefighter protective garments.

This paper investigates the impact of sunlight exposure on the mechanical properties of Twaron CT 747 para-aramid fabric samples, which were manufactured using VARTM, autoclave, and hot-pressing technologies. The aim of this study was to compare how prolonged exposure to sunlight affects the tensile and flexural characteristics of the composites.

2 EXPERIMENTAL METHODOLOGY

2.1 Materials

For the evaluation of the mechanical properties of the samples, Twaron CT 747 para-aramid fabric (Teijin Aramid, Netherlands) with a plain weave structure was used. The material datasheet for this fabric is provided in Table 1.

Reinforcement material	Weave type	Areal density (g/m ²)	Warp/Weft count (yarns/cm)	Linear density (dtex)	Thickness (mm)
------------------------	------------	-----------------------------------	----------------------------	-----------------------	----------------

Twaron CT 747	Plain	410	63	3,360	0.62
---------------	-------	-----	----	-------	------

Table 1. Material characterization of Twaron CT 747 fabric

2.2 Composite Samples Production

Composite samples A, B, and C were fabricated using the VARTM method, autoclave technology, and hot-pressing technology. All samples were manufactured using Twaron CT 747 fabric with a plain weave structure and a (0/90) ply configuration.

In the VARTM process, Twaron CT 747 fabric was positioned within a mold. The matrix comprised LG700 epoxy resin and HG700 hardener in a weight ratio of 100:30. The impregnation process was conducted under vacuum conditions. Samples A were cured at 23 °C for 24 hours. Due to the flow-driven nature of the process, local deviations in fiber distribution occurred, particularly in regions where the resin flow was influenced by fabric permeability and stacking. These variations resulted in differences in the fiber volume fraction within the sample.

Composite samples of type B were manufactured using an autoclave (Maroso, Italy). The fabrication process employed Twaron CT 747 ER68 fabric, pre-impregnated with a thermosetting resin ER68. The fiber volume fraction within the fabric was 80%. The curing process was conducted under precisely controlled conditions: the heating rate was set at 2.5 °C/min, the curing temperature was maintained at 120 °C, the autoclave chamber pressure during curing was held at 5 bar, and the total curing duration was 60 minutes. Following the completion of the curing cycle, the samples were subjected to a controlled cooling rate of 1 °C/min.

The final technique employed for the fabrication of composite samples of type C was hot-pressing. Twaron CT 747 TH110 fabric, pre-impregnated with thermoplastic polyolefin TH110, was utilized. The fiber volume fraction of the reinforcing phase was maintained at 80%. The pressing process was performed using a ZD40 laboratory press (Brno, Czech Republic). The pressing temperature was precisely controlled at (140 ± 2) °C, with a compressive force of 300 kN applied for a duration of 15 minutes. Following the completion of the pressing cycle, the material was subjected to a cooling rate of 12 °C/min. Compared to VARTM, the pre-impregnated nature of the material minimized resin-rich areas and ensured a more consistent fiber arrangement throughout the laminate.

2.3 Mechanical properties

The mechanical properties of composite samples A, B, and C were evaluated using uniaxial tensile tests and flexural tests.

Uniaxial tensile tests were performed using an Instron 5985 universal testing machine (Instron, USA), in accordance with the EN ISO 527-1 standard. The initial gauge length of the samples was set to 115 mm, with a testing speed of 5 mm/min. The dimensions of the composite samples were 250 mm × 25 mm × 2.5 mm. During testing, the tensile stress-strain curve was recorded.

Flexural tests were conducted using a Zwick Z100 testing machine (ZwickRoell, Germany) in accordance with the EN ISO 178 standard. The flexural test speed was set to 2 mm/min. The dimensions of the composite samples were 80 mm × 15 mm × 5 mm. During these tests, the flexural stress-strain curve was recorded.

As part of the evaluation, reference composite samples A, B, and C, as well as samples exposed to solar radiation, were examined.

The failure analysis of composite samples subjected to uniaxial tensile tests and flexural tests was conducted utilizing a Tescan MIRA4 scanning electron microscope (Tescan, Czech Republic).

2.4 Exposure in a climate chamber

To simulate the degradation effects of laboratory sunlight exposure, composite samples were initially dried in a drying oven in accordance with the requirements of EN ISO 62. Following the drying process, the samples were placed in a Q-SUN Xe 3HS climatic chamber (Q-Lab Corporation, USA). A Daylight filter, with a wavelength range of 295 nm to 800 nm, was selected to induce the degradation. The xenon lamps were operated at a power output of 100 W. The temperature within the climatic chamber was maintained at 60 °C, while the black panel temperature reached 90 °C. The relative humidity within the chamber was set to 25%. The degradation cycle was conducted in compliance with EN ISO 4892-2, comprising a light phase lasting 3.8 hours, followed by a dark phase with spraying, which lasted 1.2 hours. The exposure to simulated sunlight degradation was performed over periods of 31 and 122 days. The degradation effects of sunlight exposure were evaluated by measuring the weight loss of the samples. The weight loss was calculated using the equation:

$$WL = \frac{w_0 - w_1}{w_0} \times 100\% , \quad (1)$$

where WL is the weight loss (%), w_0 is the initial weight of the sample before exposure (g), and w_1 is the current weight of the sample after exposure (g).

3 RESULTS AND DISCUSSION

This chapter evaluates and discusses the mechanical properties of the reference composite samples A, B, and C, as well as the samples exposed to sunlight for 31 days and 122 days.

3.1 Mechanical properties of the reference composite samples

Figure 1 shows the representative stress-strain curve for tensile testing and the stress-deformation curve for flexural testing of the reference samples A, B, and C. Five composite samples were tested for each manufacturing technology.

The stress-strain curve (see Figure 1a) is divided into three phases. In the initial phase, the samples A and B exhibited nearly linear elastic behavior. For the composite samples C, nonlinearity was observed in the form of crimping, which was caused by the straightening of fibers. The second phase marked a transition to a non-linear elastic regime. The third phase characterized the behavior of the samples after reaching the ultimate state. In the region of maximum strength, samples A, B, and C exhibited unstable crack propagation between individual layers. This phenomenon manifested as abrupt discontinuous changes. Following the ultimate state, a reduction in tensile stress was observed.

The flexural stress-strain curve (Figure 1b) can similarly be divided into three phases. In the initial phase, samples A, B, and C exhibited a nearly linear elastic response. The second phase involved a transition to a nonlinear elastic regime. In the third phase, delamination occurred, followed by a reduction in stress after reaching the ultimate state.

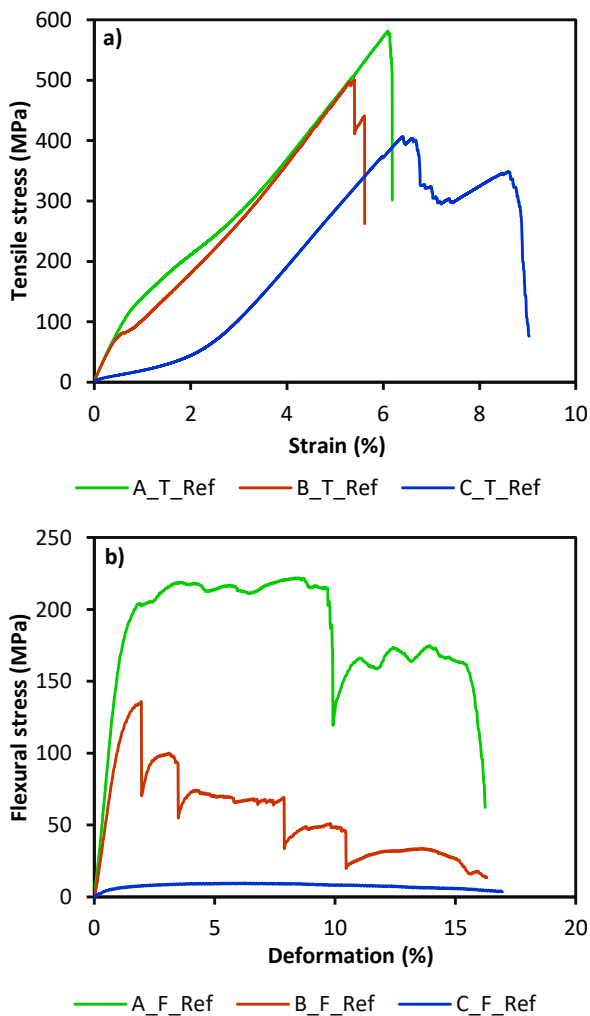


Figure 1. Mechanical properties of the reference samples A, B, and C: a) tensile stress-strain curve; b) flexural stress-strain curve

The results of the mechanical properties for the reference samples A, B, and C are summarized in Table 2. Table 2 presents the average values of tensile strength, flexural strength, tensile modulus, and flexural modulus for the reference samples A, B, and C.

Sample	Tensile strength (MPa)	Tensile modulus (GPa)	Flexural strength (MPa)	Flexural modulus (GPa)
A_Ref	586.4 ± 11.2	18.1 ± 0.9	221.8 ± 5.2	20.1 ± 1.2
B_Ref	492.8 ± 10.5	12.9 ± 0.7	139.0 ± 3.8	14.7 ± 0.8
C_Ref	399.6 ± 8.3	9.5 ± 0.6	9.9 ± 0.4	0.9 ± 0.1

Table 2. Tensile and flexural characteristics of Twaron CT 747 samples

The mechanical properties of composite samples fabricated through various manufacturing processes exhibit substantial variations, highlighting the significant influence of the production method on the material characteristics. Sample A (VARTM) demonstrates superior values for tensile strength, tensile modulus, flexural strength, and flexural modulus. Specifically, the tensile strength of sample A is 16% higher than that of sample B (autoclave technology), while sample C (hot-pressing) exhibits a 32% reduction in tensile strength compared to sample A. The difference in tensile modulus is even more pronounced, with sample A showing a 29% increase over sample B and a 47% increase over sample C. Moreover, the flexural strength of sample A is 37% higher than that of sample B and 95% higher than that of sample C. Similarly, the

flexural modulus of sample A is 27% higher than that of sample B and 95% higher than that of sample C. These results emphasize the critical role of manufacturing technologies in determining the mechanical properties of composite materials.

3.2 Exposure in a climate chamber

The weight loss of composite samples A, B, and C due to solar radiation exposure was determined using equation (1), following the EN ISO 4892-2 standard. Figure 2 shows the weight losses of the composite samples after exposure to solar radiation for 31 days and 122 days.

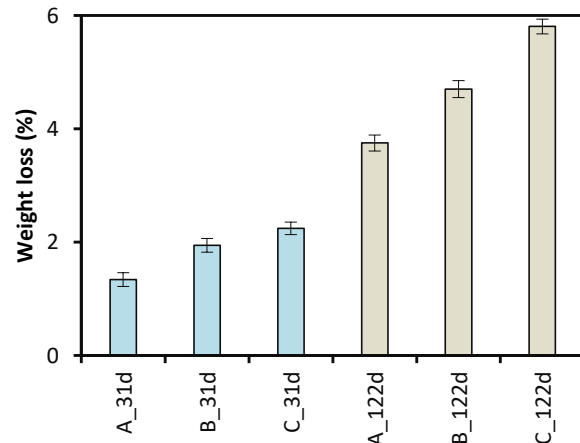


Figure 2. Weight losses of samples after exposure to solar radiation (31 days and 122 days)

Figure 2 shows that with the increasing exposure time to solar radiation, all samples exhibited significant weight losses. After 31 days of exposure, sample A exhibited the lowest weight loss, while sample B showed a 45.1% higher weight loss. Sample C had a weight loss 67.5% higher than that of sample A. After 122 days, sample B had a 25.3% higher weight loss compared to sample A, while sample C experienced a 54.8% increase. These results indicate that sample A demonstrated the lowest weight loss due to exposure to solar radiation.

3.3 Mechanical properties of composite samples after solar radiation degradation

Table 3 presents the average values of tensile and flexural characteristics for samples A, B, and C after 31 days and 122 days of solar radiation exposure.

Sample	Tensile strength (MPa)	Tensile modulus (GPa)	Flexural strength (MPa)	Flexural modulus (GPa)
A_31d	544.8 ± 9.7	15.7 ± 0.6	211.7 ± 3.3	17.2 ± 0.8
B_31d	468.3 ± 8.5	10.4 ± 0.8	129.1 ± 4.6	12.7 ± 0.7
C_31d	383.1 ± 6.2	8.3 ± 0.4	7.2 ± 0.5	0.8 ± 0.1
A_122d	410.2 ± 8.4	14.2 ± 0.3	200.3 ± 4.9	13.7 ± 0.5
B_122d	335.0 ± 9.9	9.1 ± 0.2	102.8 ± 3.5	9.0 ± 0.4
C_122d	276.7 ± 10.3	6.9 ± 0.3	2.6 ± 0.3	0.3 ± 0.1

Table 3. Tensile and flexural characteristics of samples A, B, and C after solar radiation exposure

Figure 3 compares the tensile and flexural characteristics of reference samples A, B, and C with those of samples exposed to solar radiation for 35 days and 141 days.

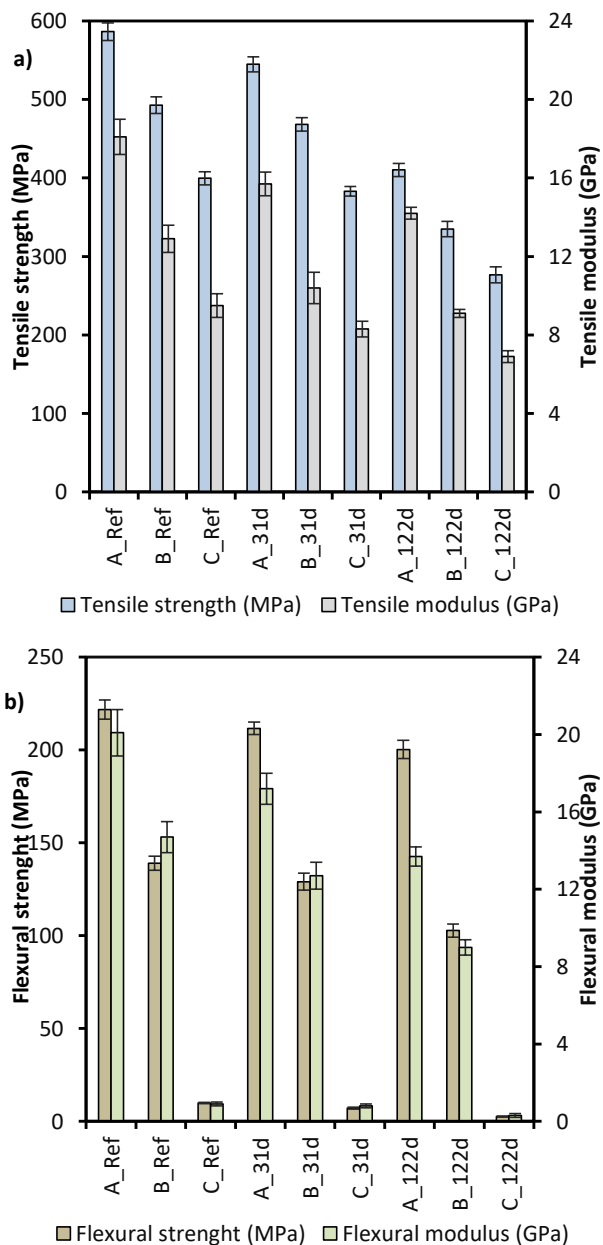


Figure 3. Comparison of mechanical properties of samples A, B, and C: (a) tensile characteristics; (b) flex-ural characteristics

Figure 3 demonstrates that, after 31 days of solar exposure, all samples exhibited a decline in tensile characteristics. Sample A showed a reduction in tensile strength, with a decrease of 13.7% compared to the reference condition. In contrast, sample B exhibited a 19.4% reduction, while sample C experienced a more substantial decrease of 26.8%. After 122 days of exposure, the tensile strength of sample A decreased by 29.6%, that of sample B by 35.2%, and sample C by 45.7%. A similar trend was observed in the tensile modulus, with the greatest degradation occurring in sample C. After 122 days, the tensile modulus of sample A decreased by 38.4%, sample B by 44.1%, and sample C by 51.9%.

The degradation of flexural characteristics was even more pronounced. After 31 days of exposure, the flexural strength of sample A decreased by 20.8%, while sample B exhibited a reduction of 32.5%, and the most significant degradation was observed in sample C, where the decrease reached 39.7%. After 122 days, the flexural strength of sample A had decreased by 45.3%, that of sample B by 54.6%, and that of sample C by 61.8%. A similar degradation trend was observed for the flexural modulus. After 122 days, the flexural modulus of

sample A had decreased by 47.2%, that of sample B by 52.8%, and that of sample C by 58.5%.

Following the tensile and flexural testing of the composite samples made from Twaron CT 747 para-aramid, a detailed analysis of the failure mechanisms was conducted using scanning electron microscopy. Figure 4 illustrates representative fracture surfaces of the composite sample C_Ref.

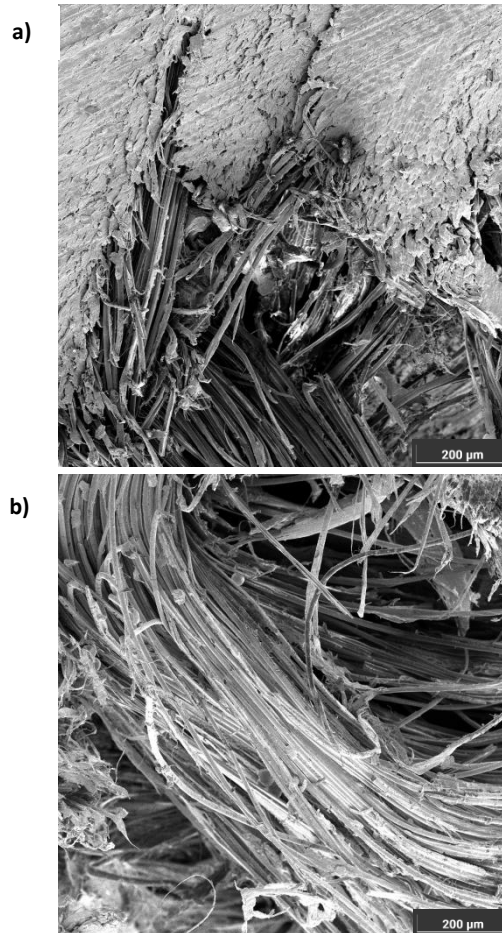


Figure 4. Fracture surface C_Ref: (a) SEM, magnification 560x; (b) SEM, magnification 560x

In the tensile test (Figure 4a), it was observed that the failure of the samples was primarily caused by delamination of the individual layers, which was attributed to low adhesion between the fibers and the matrix. During the tensile test, matrix cracking was recorded, leading to fiber stretching. This process subsequently caused shear failure of the fibers. The failure mechanisms of the samples in the flexural test exhibited similar characteristics to those observed in the tensile test. In Figure 4(b), failure mechanisms were identified, involving both flexural and tensile deformation processes. The delamination area of the sample visible in Figure 4(b) suggests the presence of tensile stress at the bottom of the sample and compressive stress at the top.

4 CONCLUSIONS

This study analyzed the effect of exposure to solar radiation on the mechanical properties of composite materials made from Twaron CT 747 para-aramid fiber, comparing three manufacturing technologies: VARTM, autoclave, and hot-pressing.

The results demonstrated that the degradation of mechanical properties is significantly influenced by the manufacturing

method used. The highest initial tensile strength was measured in samples produced using the VARTM method, while autoclaved samples exhibited lower strength, and hot-pressed samples showed the lowest values. After 122 days of exposure to solar radiation, tensile strength decreased by 29.6% for VARTM samples, 35.2% for autoclaved samples, and 45.7% for hot-pressed samples. A similar trend was observed in flexural strength, which decreased by 45.3% for VARTM samples, 54.6% for autoclaved samples, and the most significant degradation of 61.8% was observed in the hot-pressed samples. Scanning electron microscopy confirmed extensive delamination and the formation of microcracks, which were most pronounced in the hot-pressed samples.

The key contribution of this study lies in the systematic comparison of different manufacturing techniques and their influence on the mechanical degradation of composite materials exposed to prolonged solar radiation.

ACKNOWLEDGMENTS

The work presented in this paper was supported by the specific research projects "SV23-216" and "SV24-216" at the Department of Mechanical Engineering, University of Defence in Brno and was supported by the Project for the Development of the Organization "VAROPS (DZRO VAROPS) Military autonomous and robotic assets" by the Ministry of Defence of Czech Republic.

REFERENCES

- [Sharma 2023] Sharma, H., et al. Critical review on advancements on the fiber-reinforced composites: Role of fiber/matrix modification on the performance of the fibrous composites. *Journal of Materials Research and Technology*, 2023, Vol.26, pp 2975–3002, ISSN 2238-7854. <https://doi.org/10.1016/j.jmrt.2023.08.036>
- [Arulprasanna 2024] Arulprasanna, A. and Omkumar, M. A review on composites: Selection and its applications. *Materials Today: Proceedings*, 2024, (in press), ISSN 2214-7853. <https://doi.org/10.1016/j.matpr.2024.06.014>
- [Sumithra 2023] Sumithra, G., et al. Review on composite classification, manufacturing, and applications. *Materials Today: Proceedings*, 2023, (in press), ISSN 2214-7853. <https://doi.org/10.1016/j.matpr.2023.04.637>
- [Mechali 2024] Mechali, A., et al. Research about M300 Maraging Steel Metallic Powder for Use in SLM 3D Printing. *MM Science Journal*, October 2024, pp 7569 - 7575. https://doi.org/10.17973/MMSJ.2024_10_2024080
- [Saharudin 2021] Saharudin, M.S., et al. Quality of Surface Texture and Mechanical Properties of PLA and PA-Based Material Reinforced with Carbon Fibers Manufactured by FDM and CFF 3D Printing Technologies. *Polymers*, 2021, Vol.13, No.11, pp 1671. <https://doi.org/10.3390/polym13111671>
- [Chaudhary 2024] Chaudhary, B., et al. Review of fiber-reinforced composite structures with multifunctional capabilities through smart textiles. *Textiles*, 2024, Vol.4, No.3, pp 391-416. <https://doi.org/10.3390/textiles4030023>
- [Sharma 2020] Sharma, A. K., et al. Matrix materials used in composites: A comprehensive study. *Materials Today: Proceedings*, 2020, Vol.21, pp 1559–1562. <https://doi.org/10.1016/j.matpr.2019.11.086>
- [Mahboubizadeh 2024] Mahboubizadeh, S., et al. Advancements in fiber-reinforced polymer (FRP) composites: An extensive review. *Discover Materials*, 2024, Vol.4, No.1, pp 22. ISSN 2731-996X. <https://doi.org/10.1007/s43939-024-00091-9>
- [Sajan 2021] Sajan, S. and Philip Selvaraj, D. A review on polymer matrix composite materials and their applications. *Materials Today: Proceedings*, 2021, Vol.47, pp 5493–5498, ISSN 2214-7853. <https://doi.org/10.1016/j.matpr.2021.08.034>
- [Xiao 2024] Xiao, Y., et al. Mechanical properties of aramid fiber fabrics and composites enhanced by phthalic anhydride catalyzed with anhydrous aluminum chloride. *Applied Sciences*, 2024, Vol.14, No.9, pp 3800. <https://doi.org/10.3390/app14093800>
- [Dharmavarapu 2022] Dharmavarapu, P. and M.B.S, S. R. Aramid fibre as potential reinforcement for polymer matrix composites: A review. *Emergent Materials*, 2022, Vol.5, No.5, pp 1561-1578. <https://doi.org/10.1007/s42247-021-00246-x>
- [Talikota 2019] Talikota, R. S. and Kandekar, S. B. Strength and durability study of concrete structures using aramid-fiber-reinforced polymer. *Fibers*, 2019, Vol.7, No.2, pp 11. <https://doi.org/10.3390/fib7020011>
- [Vilis 2024] Vilis, J., et al. Influence of water absorption on tensile and flexural properties of composite samples. In *Metal* 2024, pp. 461–466.
- [Santos 2023] Santos, T., et al. Effects of UV sensitivity and accelerated photo-aging on stab resistance of p-aramid fabrics impregnated with shear thickening fluids (STFs). *Heliyon*, 2023, Vol.9, No.4, pp e15020. <https://doi.org/10.1016/j.heliyon.2023.e15020>
- [Wakatsuki 2022] Wakatsuki, K., et al. Effects of m-Aramid/p-Aramid blend ratio on tensile strength due to UV degradation for firefighter clothing fabrics and development of predictive equation for tensile strength. *Polymers*, 2022, Vol.14, No.16, pp 3241. <https://doi.org/10.3390/polym14163241>

CONTACTS:

Ing. Jindrich Vilis
University of Defence, Faculty of Military Technology, Department of Mechanical Engineering
Kounicova 65, 662 10 Brno, Czech Republic
jindrich.vilis@unob.cz, <https://unob.cz/>